Determinants of Enzyme Thermostability Observed in the Molecular Structure of *Thermus aquaticus* D-Glyceraldehyde-3-phosphate Dehydrogenase at 2.5 Å Resolution[†,‡]

John J. Tanner, Ralph M. Hecht, and Kurt L. Krause*

Department of Biochemical and Biophysical Sciences, University of Houston, Houston, Texas 77204-5934

Received August 21, 1995; Revised Manuscript Received November 22, 1995[⊗]

ABSTRACT: The crystal structure of holo D-glyceraldehyde-3-phosphate dehydrogenase (GAPDH) from the extreme thermophile *Thermus aquaticus* has been solved at 2.5 Å resolution. To study the determinants of thermostability, we compare our structure to four other GAPDHs. Salt links, hydrogen bonds, buried surface area, packing density, surface to volume ratio, and stabilization of α-helices and β-turns are analyzed. We find a strong correlation between thermostability and the number of hydrogen bonds between charged side chains and neutral partners. These charged-neutral hydrogen bonds provide electrostatic stabilization without the heavy desolvation penalty of salt links. The stability of thermophilic GAPDHs is also correlated with the number of intrasubunit salt links and total hydrogen bonds. Charged residues, therefore, play a dual role in stabilization by participating not only in salt links but also in hydrogen bonds with a neutral partner. Hydrophobic effects allow for discrimination between thermophiles and psychrophiles, but not within the GAPDH thermophiles. There is, however, an association between thermostability and decreasing enzyme surface to volume ratio. Finally, we describe several interactions present in both our GAPDH and a hyperthermophilic GAPDH that are absent in the less thermostable GAPDHs. These include a four-residue salt link network, a hydrogen bond near the active site, an intersubunit salt link, and several buried Ile residues.

The question of why proteins are stable is of fundamental importance in biochemistry. It is a crucial issue in the designing of enzymes for industrial and medical applications that function under extreme environmental conditions. It is also central to understanding the relationship between amino acid sequence and three-dimensional structure, and ultimately in the prediction of a protein's structure from its sequence.

The crystal structures of proteins from thermophilic microorganisms have contributed to our understanding of the principles underlying thermostability (Day et al., 1992; Davies et al., 1993; Kelly et al., 1993; Chan et al., 1995; Korndörfer et al., 1995). We report the 2.5 Å crystal structure of holo D-glyceraldehyde-3-phosphate dehydrogenase (GAPDH)[1] from the extreme thermophile *Thermus aquaticus* (TA). This structure was solved using molecular replacement and noncrystallographic symmetry (NCS) averaging.

High- and medium-resolution structures of GAPDHs from several organisms are already known, including the psychrophilic lobsters *Homarus americanus* (HA) (Moras et al., 1975; Murthy et al., 1980) and *Palinurus versicolor* (Lin et al., 1993), the moderate thermophile *Bacillus stearothermophilus* (BS) (Skarzynski et al., 1987; Skarzynski & Wonacott, 1988), and the hyperthermophile *Thermotoga maritima* (TM) (Korndörfer et al., 1995). There are also low-resolution structures of GAPDH from human skeletal muscle (Mercer et al., 1976), *Bacillus coagulans* (Griffith et al., 1983), and *Trypanosoma brucei* (Vellieux et al., 1993).

With the report of the TA structure, there are now four GAPDH structures of medium to high resolution that span a broad range of thermostability; therefore, we are in a unique position to look for the basis of their relative thermostability. The thermostability of TA is intermediate among those of known structure. It exhibits a half-life of 30 min at 100 °C (Tanner et al., 1994), whereas both HA and BS are rapidly denatured at this temperature (Suzuki & Harris, 1971). TM is even more thermostable than TA, with a half-life at 100 °C of 60 min (Rehaber & Jaenicke, 1992).

Much research has been devoted to determining which forces are responsible for thermostability, including studies of thermostable GAPDHs (Fabry et al., 1989; Biro et al., 1990; Zwickl et al., 1990; Tomschy et al., 1993, 1994; Jecht et al., 1994) and other enzymes from thermophiles (Zuber, 1981; Honka et al., 1990; Jaenicke, 1991; Schläpfer & Zuber, 1992; Kotik & Zuber, 1993; Adams & Kelly, 1994; Knapp et al., 1995; Rees & Adams, 1995; Sterner et al., 1995; Yip et al., 1995), site-specific mutagenesis studies (Alber, 1989; Matthews, 1991, 1995), double mutant cycle experiments (Fersht & Serrano, 1993), amino acid sequence analysis

[†] This work was supported by the National Science Foundation (to R.M.H.), the U.S. Army Research Office (to R.M.H.), the National Institutes of Health (to K.L.K.), the W. M. Keck Foundation, and the Institute for Molecular Design. Some equipment and computers used in this research were purchased with grants provided by the National Science Foundation.

[‡] Coordinates have been deposited in the Brookhaven Protein Data Bank under ID Code 1CER.

* Corresponding author. Email: kkrause@uh.edu.

[⊗] Abstract published in *Advance ACS Abstracts,* February 1, 1996.

[1] Abbreviations: GAPDH, D-glyceraldehyde-3-phosphate dehydrogenase; HA, *Homarus americanus* GAPDH; HAH, holo *Homarus americanus* GAPDH; HAA, apo *Homarus americanus* GAPDH; BS, holo *Bacillus stearothermophilus* GAPDH; TA, holo *Thermus aquaticus* GAPDH; TM, holo *Thermotoga maritima* GAPDH; RMSD, root mean square differences; NCS, noncrystallographic symmetry; A_s, solvent-accessible surface area.

0006-2960/96/0435-2597$12.00/0

(Perutz & Raidt, 1975; Argos et al., 1979; Merkler et al., 1981; Menendez-Arias & Argos, 1989), and electrostatics calculations (Yang et al., 1992; Hendsch & Tidor, 1994; Honig & Nicholls, 1995). Several factors have been shown to have an effect on the thermostability of a protein, including salt links, hydrogen bonds, hydrophobic interactions, internal packing, stabilization of helices, and strategic placement of Pro in β-turns. Despite this large body of work, however, there is disagreement over which is the dominant force in stabilizing proteins, whether salt links and hydrogen bonds are stabilizing or destabilizing, and whether surface salt links are more or less stabilizing than buried salt links.

We present the new structure of a GAPDH from an extreme thermophile and compare it to the structures of GAPDHs from a psychrophile (HA), a moderate thermophile (BS), and a hyperthermophile (TM). We compare these GAPDHs in terms of salt links, hydrogen bonds, packing density, buried and exposed surface area, surface to volume ratio, stabilization of helix dipoles, and occurrence of Ala in α-helices and Pro in β-turns. We also identify residues crucial for thermostability on the basis of sequence conservation in the two most thermostable GAPDHs, TA and TM.

MATERIALS AND METHODS

Crystallization and X-ray Data Collection. Purification, crystallization, and space group determination of TA cloned in *Escherichia coli* were described elsewhere (Tanner et al., 1994). The enzyme was crystallized using a mixture of poly(ethylene glycol) and 2-propanol at pH 8.4. The space group is $P2_12_12_1$ with cell dimensions $a = 144.8$ Å, $b = 148.8$ Å, $c = 149.5$ Å. The asymmetric unit contains two tetramers.

A 2.5 Å data set was collected on an R-axis II imaging plate coupled to a Siemens rotating anode operated at 50 kV and 90 mA with a 0.3 mm collimator. The detector θ angle was 0°, and the detector distance was 150 mm. A total of 125 frames were collected with a frame width of 1°. Standard Rigaku R-axis software was used to collect and process the data (Higashi, 1990). Several data processing trials were performed to find a scheme that would produce the best possible data (Tanner & Krause, 1994). The final data set was processed using postrefinement of the crystal mosaicity, followed by reintegration of the frame data and slip check. It contains 267 328 observations of 81 628 unique reflections and has a merging *R*-factor of 5.65%. The merging *R*-factors for full and partial reflections are 5.43% and 5.80%, respectively. This data set is 72% complete to 2.5 Å and 83% complete to 2.7 Å. The 2.6−2.5 Å shell of data is 30% complete.

Molecular Replacement. Rotation and translation functions were calculated with X-PLOR version 3.1 (Brünger, 1992) using 6−4 Å data. The search model was the BS tetramer, with NAD^+, water, and SO_4 removed. The TA sequence is 63% identical to the BS sequence. The P, Q, and R molecular axes of the search model were coincident with the *x*, *y*, and *z* axes, respectively, and the centroid was (0,0,0).

Rotation function and Patterson correlation calculations revealed that both tetramers in the asymmetric unit have their Q molecular axes approximately coincident with the crystallographic *a* axis (Tanner et al., 1994). The orientations of the two tetramers obtained from the rotation functions are listed in Table 1. The tetramers are named according to the labeling of their subunits, with tetramer OPQR comprising subunits O, P, Q, R, and tetramer ABCD comprising subunits A, B, C, D.

Table 1: Final Results of Molecular Replacement

	orientation (Euler angles)			position (fractional)		
tetramer	θ_1	θ_2	θ_3	*x*	*y*	*z*
OPQR	91.32	48.43	7.67	0.222	0.002	0.070
ABCD	276.44	40.30	182.12	0.246	0.494	0.039

The location of tetramer OPQR was determined from a translation function calculated on a 2.0 Å grid. The highest peak had height 18 σ. Next, the location of tetramer ABCD was found from a 2.5 Å grid translation function with tetramer OPQR also contributing to the calculated structure factors. The highest peak of this search had height 30 σ. The locations of the two tetramers were then refined from local translation functions calculated on a 0.5 Å grid. The final *R*-factor was 43% for 6−4 Å data. The final positions of the two tetramers are listed in Table 1.

Refinement and Model Building. The search model used in molecular replacement was modified by mutating residues not conserved by BS and TA to either Ala or Gly and setting the *B*-factors to 18 Å^2 (average *B*-factor of BS structure). Two loops of the search model contain deletion sites (Asp 24 and Asp 301 in BS). These regions were handled by omitting residues 18−30 and 298−303 from the initial model and gradually building these loops into difference density. Residue 0 Ala was deleted from the search model.

The modified search model was replicated and the two tetramers positioned according to the transformations in Table 1. Rigid-body refinement was performed in two stages with X-PLOR using 10−3 Å data. In the first stage, the two tetramers were considered to be rigid bodies, and in the second stage, all eight subunits were allowed to move. Rigid-body refinement lowered the *R*-factor to 38.5% for 10−3.0 Å data. Electron density maps showed strong difference density for all eight NAD^+ molecules.

Positional refinement was done using X-PLOR conjugate gradient minimization with the Engh and Huber force field (Engh & Huber, 1991) and strict NCS on a Cray YMP/EL. NCS averaging and solvent flattening calculations were performed with the PHASES program package (Furey & Swaminathan, 1995), as was refinement of the NCS transformations. O (Jones et al., 1991) and FRODO (Jones, 1978) were used for model building. OOPS (Jones et al., 1991) was used to search for problematic residues. The stereochemistry of the model was evaluated with PROCHECK (Laskowski et al., 1993).

The first few rounds of refinement were carried out with strict 8-fold NCS constraints at 6.5−3.0 Å resolution. The first round of positional refinement reduced the *R*-factor to 31.9% for 6.5−3.0 Å data. Missing side chains were built into difference density, and the NCS averaged, solvent flattened maps helped guide rebuilding sessions. Following data extension to 2.5 Å resolution, NAD^+ was built into difference density, and individual *B*-factors were refined using restraints to standard deviations of 1.0 Å^2 for main chain bonded atoms, 1.5 Å^2 for side chain bonded atoms, 1.5 Å^2 for main chain atoms related by bond angles, and 2.0 Å^2 for side chain atoms related by bond angles. After the *R*-factor reached 23.4% for 6.5−2.5 Å data, the 8-fold strict

Table 2: Data Used To Determine Correct NCS Relation

NCS relation (rotational part)	correlation coefficient	*R*-factor
−90° about *a*	0.93	24.0
90° about *a*	0.89	24.4
180° about *b*	0.88	24.3
180° about *c*	0.94	23.8

NCS constraint was relaxed to 2-fold averaging between the two tetramers.

The use of 2-fold strict NCS in the final model necessitated resolution of an ambiguity concerning the NCS transformation relating the two tetramers. This ambiguity arises from the symmetry of the tetramer. Since the tetramer has approximate *222* symmetry, there are four choices for the transformation that takes tetramer OPQR to tetramer ABCD. One choice is simply the transformation returned by the rotation functions, i.e., an approximate −90° rotation around *a*. The other choices are generated by following the −90° rotation around *a* with rotations around each of the molecular 2-fold axes. The resultant net rotations are −90° around *a*, 90° around *a*, 180° around *b*, and 180° around *c*. Note that the first two rotations are equivalent in a self-rotation function performed in *P222* since they are related by a 2-fold rotation around *a*. Likewise, the latter two rotations are related to the origin peak by rotation symmetry. Since the tetramer does not possess exact *222* symmetry, the choice is not arbitrary, and one transformation is likely to be more accurate than the others when used in NCS averaging.

Two tests were designed to determine the correct transformation. First, we refined the four possible NCS relations and compared the final electron density correlation coefficients. Second, each NCS relation was used in a separate conjugate gradient refinement with strict NCS symmetry, and the final *R*-factors compared. The results of these tests are in Table 2. The NCS relation that produced both the highest correlation coefficient and the lowest *R*-factor is the 2-fold rotation around *c*, so this transformation was used in subsequent strict NCS conjugate gradient refinement and NCS averaging calculations.

The refined NCS transformation that generates tetramer ABCD from tetramer OPQR is a spherical polar rotation of $\psi = 93.83°$, $\phi = 92.24°$, $\kappa = 181.74°$, followed by a translation of $x = 66.57$ Å, $y = 73.23$ Å, $z = -7.53$ Å. After several rounds of refinement using strict 2-fold NCS followed by rebuilding and addition of missing side chains, the data were extended in the low-resolution direction to 12 Å with the use of a bulk solvent mask.

Analysis. Analyses of salt links, hydrogen bonds, solvent-accessible surface area (A_s), and root mean square differences (RMSD) were done with X-PLOR. The probe radius for A_s calculations was 1.4 Å, and the X-PLOR numerical accuracy parameter was set to 0.025. GRASP (Nicholls & Honig, 1992) was used to calculate properties related to the molecular surface, such as the surface to volume ratio and the packing density. The probe radius used in GRASP was 1.4 Å, and the surface resolution parameter was set to 1.8.

The following GAPDH structures, which were obtained from the protein data bank (Abola et al., 1987), were used in our analyses: HA holo form (HAH) (entry id 1GPD; Moras et al., 1975), HA apo form (HAA) (entry id 4GPD; Murthy et al., 1980), BS (entry id 1GD1; Skarzynski et al., 1987), and TM (entry id 1HDG; Korndörfer et al., 1995). The complete tetramer is included in the HAA and BS entries. Crystallographic symmetry was used to build the TM tetramer from a dimer, and noncrystallographic symmetry was used to build the HAH tetramer from a dimer. All calculations were performed after removal of water molecules, NAD^+, SO_4, and heavy atoms with zero occupancy. Hydrogen atoms were added for the purpose of calculating hydrogen bonds but were omitted in all other calculations. The structure of *P. versicolor* GAPDH was not in the data bank (November, 1995); therefore, it was not included in our analysis.

RESULTS

Quality of the Model. The final structure is an NCS-averaged model of 1 tetramer, containing 10 113 atoms, including 1324 amino acid residues and 4 NAD^+ molecules. The BS residue number scheme is used. Water molecules were not added, and the phosphate sites, which are typically occupied by SO_4 in GAPDH crystals grown in ammonium sulfate, are unoccupied in this crystal form. A drawing of the TA tetramer is shown in Figure 1.

The *R*-factor of the final model is 20.5% for 80 657 reflections between 12 and 2.5 Å resolution using a bulk solvent mask and strict 2-fold NCS. The root mean square deviation from the ideal force field values is 0.021 Å for bonds and 2.3° for angles. The stereochemistry meets or exceeds all the main chain and side chain tests of the PROCHECK package (Laskowski et al., 1993). Ninety-nine percent of all non-Gly and non-Pro residues fall in either the most favorable or additional allowed regions of the Ramachandaran plot, and there are no non-Gly residues in the disallowed regions. A Luzzati plot suggests a mean positional error of about 0.30−0.35 Å (Luzzati, 1952).

A plot of the real space correlation coefficient (Jones et al., 1991) between the model (all atoms) and the NCS-averaged, solvent-flattened $|F_o|$ map is shown in Figure 2. The average correlation for the entire tetramer is 0.91, and the standard deviation is 0.026. The data in Figure 2 suggest that the weakest part of the model is residues 50−114, which is part of the NAD^+ binding domain (residues 1−148, 312−333). Inspection of the electron density confirms this suggestion. In general, the density is weaker and more diffuse in NAD^+ binding domains than in the catalytic domains. The main chain density is continuous throughout the entire tetramer, and the trace is unambiguous. Many of the residues with the weakest electron density also have high solvent exposure, particularly the 60's loop, the short helical segment containing Glu 86, and the 100−110 helix. The electron density is excellent in the catalytic domains of all four subunits, and throughout the entire Q chain. The NCS-averaged, solvent-flattened $|F_o|$ map is superimposed on a portion of the final model in Figure 3.

The average *B*-factor of all atoms is 28.6 Å^2; the average *B*-factor of main chain atoms is 28.2 Å^2. The *B*-factors of this model are higher than those found in other GAPDHs. For comparison, the average *B*-factor for all atoms in other GAPDH structures ranges from 11.0 Å^2 in HAA to 22.3 Å^2 in TM. A Wilson plot of our data suggests an overall *B*-factor of 30 Å^2 (data not shown), which is in good agreement with the model. The *B*-factors of the catalytic domain residues are generally lower than those in the NAD^+ binding domain. This trend is also observed in other

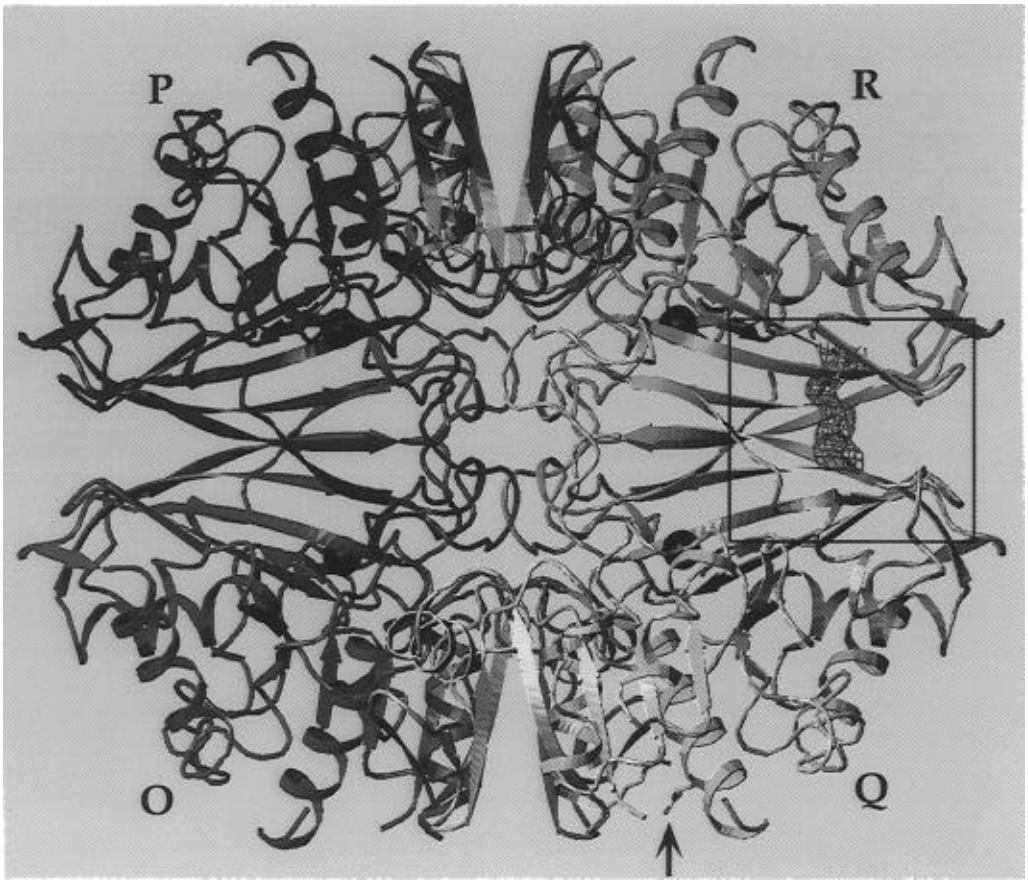

FIGURE 1: TA tetramer, with the four subunits assigned different colors. The view is down the R molecular axis with the P axis horizontal and the Q axis vertical. Black spheres of radius 1.7 Å are located at the SG atoms of the four active-site Cys 149 residues. The arrow points to the salt link between Glu Q326 and Arg Q22 that is discussed in the text and shown in detail in Figure 6a. The box highlights an intersubunit salt link that is also discussed in the text and is shown in detail in Figure 11. This drawing was prepared with O (Jones et al., 1991).

GAPDH structures, most notably in HAA, but also in TM and BS.

Since strict NCS refinement in X-PLOR excludes nonbonded forces generated by crystallographic symmetry, the model was manually inspected for bad crystal contacts. We found one region that is obviously incorrect due to a breakdown of NCS. The side chain of P138 Asp forms a bad contact with a crystallographic mate of A253 Glu. There is strong negative difference density covering the side chain of A253 and strong positive difference density indicating the correct torsion angle. A253 Glu would probably form a crystallographic salt link with P331 Lys in a model without NCS constraints. This is the only blatant violation of 2-fold NCS, although there are several minor violations in crystal contact regions. In contrast to the situation involving A253 Glu, these minor violations would probably be corrected during conjugate gradient refinement without NCS constraints; i.e., they would not require manual rebuilding.

Several side chains were truncated after the C_β atom because of weak electron density: Met 1 (OPQR), Glu 26 (OPQR), Asp 61 (OQR), Lys 69 (O), Lys 77 (OPQR), Lys 80 (OPQR), Asp 101 (OQR), Lys 106 (OPQR), Glu 135 (OPR), Ser 139 (OQR), Arg 140 (OQR), Lys 191 (O), Lys 268 (R), Arg 330 (OPQR), and Val 333 (OPQR).

Comparison to Other GAPDH Structures. (A) Overall Structure. In this section, we present a detailed comparison to the BS model because it was used as the search model for molecular replacement and has high sequence identity (63%) to TA. We also present less detailed comparisons to the HA and TM structures. For reference, an alignment of the HA, BS, TA, and TM sequences appears in Figure 4.

As expected, the secondary structure elements and overall fold of the enzyme are very similar to those of other GAPDH structures. After superimposing the TA and BS tetramers using a least-squares fit of the C_α atoms, the RMSD for C_α atoms is 0.84 Å, and the RMSD for all atoms of conserved residues is 0.95 Å. These low RMSD values suggest that we did not observe the 4.4° rigid-body rotation of the NAD^+ binding domain that was seen in the TM structure (Korndörfer et al., 1995). Despite the small overall RMSD between the two structures, some regions of the enzyme display large local RMSD. We plot the C_α RMSD for the Q subunit in Figure 5, and note that this plot is representative of the other three subunits. All four subunits display large RMSD in the regions near residues 22, 60, 82, 86, 250, and 300. We next describe the structural differences in each of these regions.

The 20's turn connects an α-helix to a β-strand. Asp 24 is present in BS but is deleted in the TA sequence. This deletion causes conformational changes in the turn. Qualitatively, the turn in TA is shorter and sharper, and there is a significant increase in the interaction between this turn and the 315−330 helix (Figure 6).

Arg 22 of TA is analogous to Lys 21 of BS, in that both are basic residues located near the beginning of the 20's loop. In TA, Arg 22 forms salt bridges with Asp 323 and Glu 326. Lys 21 in BS does not interact with the 300's helix, with a distance of 10 Å separating Lys 21 NZ and the

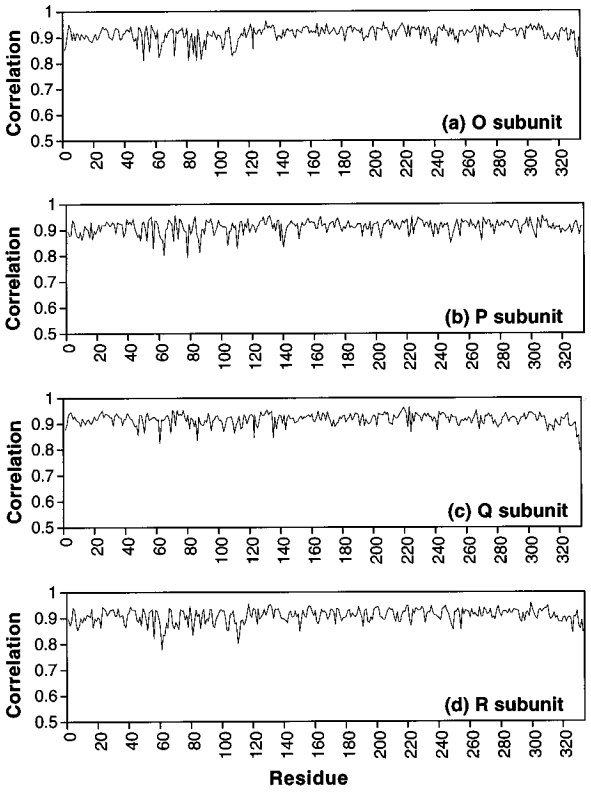

FIGURE 2: Real space correlation coefficients of the four subunits of the tetramer calculated with O (Jones et al., 1991). The correlation is between the all-atom final model and the NCS-averaged, solvent-flattened $|F_o|$ map. The O rsr−setup parameters were $A_0 = 0.9$, $C = 0.82$.

carboxylate oxygen atoms of Asp 323. The salt link between Arg 22 and Asp 323 in TA does not disrupt the Arg 320−Asp 323 salt link, which is conserved in all five structures. Rather, a four-residue salt link network involving Arg 320, Asp 323, Arg 22, and Glu 326 is formed. This network might be a source of domain stabilization. The failure of the Lys 21 in BS to make a salt link to the 300s helix is partly due to the fact that Lys is too short to bridge the gap between the 20's turn and the 300's helix. Residue 319 could also play a role (Figure 6). In BS, His 319 is in position to set up an unfavorable electrostatic field preventing Lys 21 from approaching Asp 323. In TA, residue 319 is Asn, and it hydrogen bonds to Arg 22. We tested this notion by adjusting the side chain dihedral angles of Lys 21 of BS. We were able to move the NZ to within just over 4 Å from an Asp 323 carboxylate oxygen, but this also put the NZ less than 4 Å from an imidazole nitrogen of His 319.

This four-residue salt link network is also observed in TM, but not in the HA structures. In TM, the conformations of the Arg in the 20's turn, as well as Asn 319, Arg 320, Asp 323, and Glu 326, are almost identical to those found in TA.

The 60's loop of TA is also substantially different from that in BS. This loop is a reverse turn that connects two short stretches of β-strand. Whereas the loop is somewhat kinked in BS, it is more extended in TA. The main chain hydrogen bonding patterns are also different. In BS, the i to $i+3$ hydrogen bond, which is typically found in reverse turns, is present. This hydrogen bond is absent in TA because the carbonyl of Asp 60 points out of the loop and into solvent. In its place, however, is a hydrogen bond between Asp 60 OD1 and Tyr 65 OH. The 60's turn in TM is similar to that of TA, both in conformation and in hydrogen bonding pattern. In TM, the i to $i+3$ main chain hydrogen bond is also missing, and it is replaced by a hydrogen bond between Thr 60 OG1 and Ser 63 OG. The 60's loops in the HA structures are similar to the BS loop.

The high RMSD observed at residues 83−86 is mainly due to the introduction of a Pro at position 83 in place of an Ala in BS. The electron density for the side chain of Glu 86 is weak, and there is some difference density in this area. Glu 86 is a conserved residue with high solvent exposure (77−95%), and lack of an explicit solvent model may contribute to the observed differences.

Arg 248 sits near the beginning of a turn that connects a β-strand and an α-helix, and it replaces a Lys in HA, BS, and TM. The observed differences from the BS structure in the O subunit involve the formation of a salt link between Arg 248 and Glu 254 that stretches across the length of the loop and ties the start of the loop to the helix. This salt link

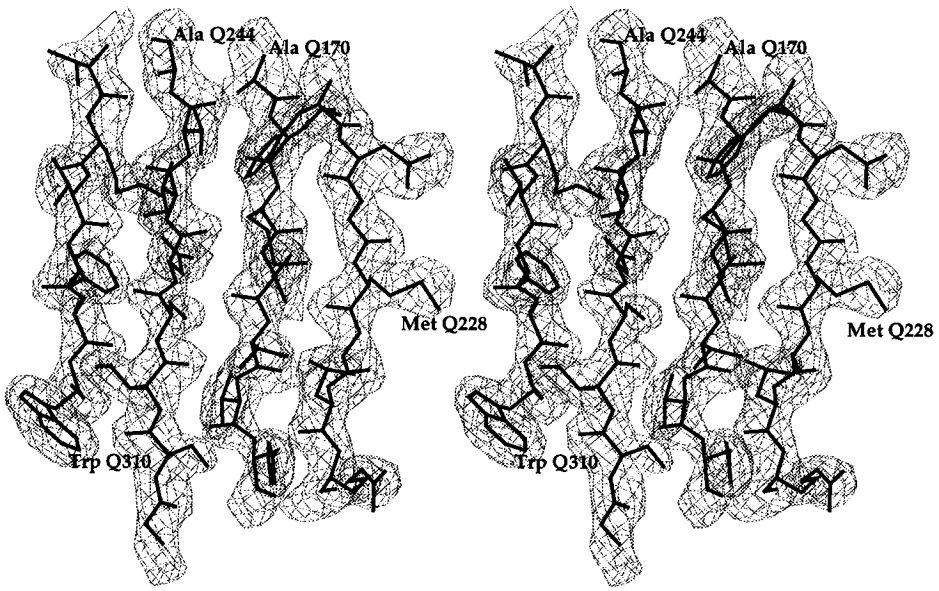

FIGURE 3: Stereoview of the NCS-averaged, solvent-flattened $|F_o|$ map (contoured at 1.25σ) superimposed on the final model. The map was calculated from observed amplitudes, $|F_o|$, and phases that were improved with 2-fold NCS-averaging and solvent-flattening. The model is part of the β-sheet region of the catalytic domain of the Q subunit.

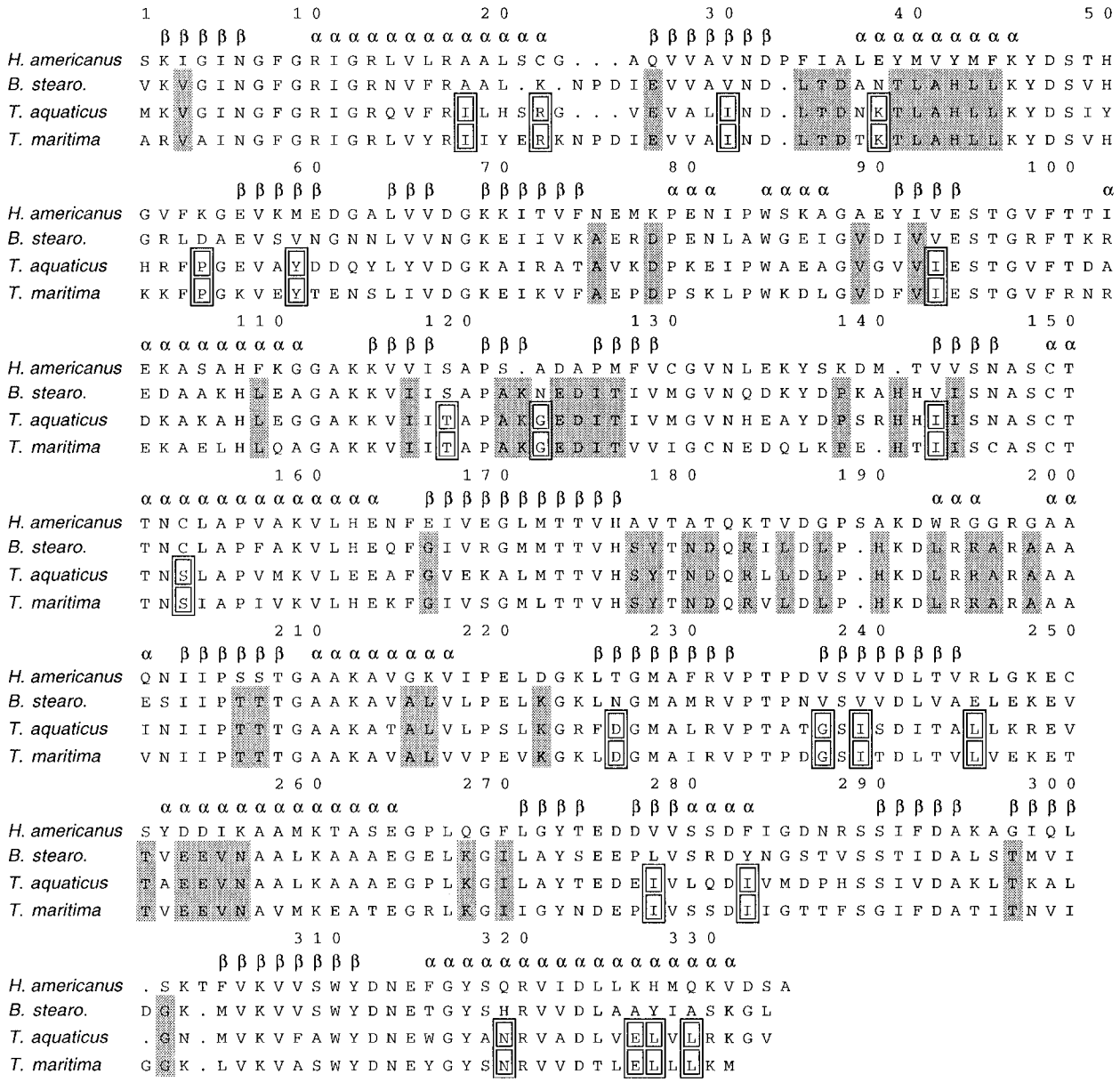

FIGURE 4: Structure-based alignments of the sequences of four GAPDHs. The sequences were aligned with GCG Bestfit (Devereux et al., 1984), and verified manually using structures superimposed by a least-squares fit of the C_α atoms. A few changes to the Bestfit alignments were made in loop regions containing insertions or deletions, such as the 20's loop and the 300's loop. The residue numbers apply to the *T. aquaticus* structure only, and they are right-justified over the residue letter. The secondary structure assignments were obtained with O (Jones et al., 1991) using the TA structure. The shaded residues are present in BS, TA, and TM, but absent in HA. The boxed residues are present only in TA and TM, and absent in HA and BS.

is not observed in the other GAPDH structures because Lys is too short to span the distance required to make the salt link.

In the other subunits of TA, however, the Arg 248−Glu 254 salt link is disrupted by crystallographic and noncrystallographic packing forces. P254 Glu forms a salt link with Q224 Arg in a crystallographically related molecule, while R254 Glu links with O224 Arg in a crystallographically related molecule. In an analogous way, Q254 Glu forms a salt link with R224 Arg in an NCS-related molecule.

Finally, the 300's turn contains a deletion site, Asp 301 in BS. In contrast to the 20's loop, the changes in this loop are isolated to a single residue, Gly 302. The conformation of the turn is close to what one would have predicted by simply cutting out Asp 301 from the BS structure, except for the conformation of Gly 302. After removal of Asp 301, the turn becomes a type II' reverse turn.

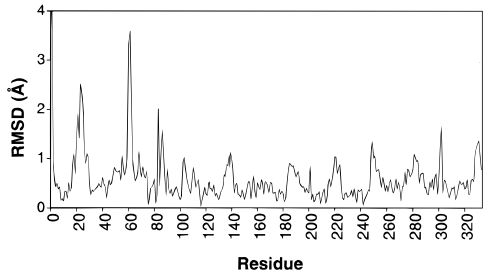

FIGURE 5: Root mean square differences between the C_α atoms of TA and BS after least-squares superposition. Data are shown for the Q subunit only, but this plot is representative of the RMSD in the other three subunits.

(B) Active Site. Cys 149 is directly involved in catalysis as the nucleophile that reacts with the aldehyde portion of the substrate, D-glyceraldehyde 3-phosphate. His 176 is thought to act as a base by extracting a proton from Cys

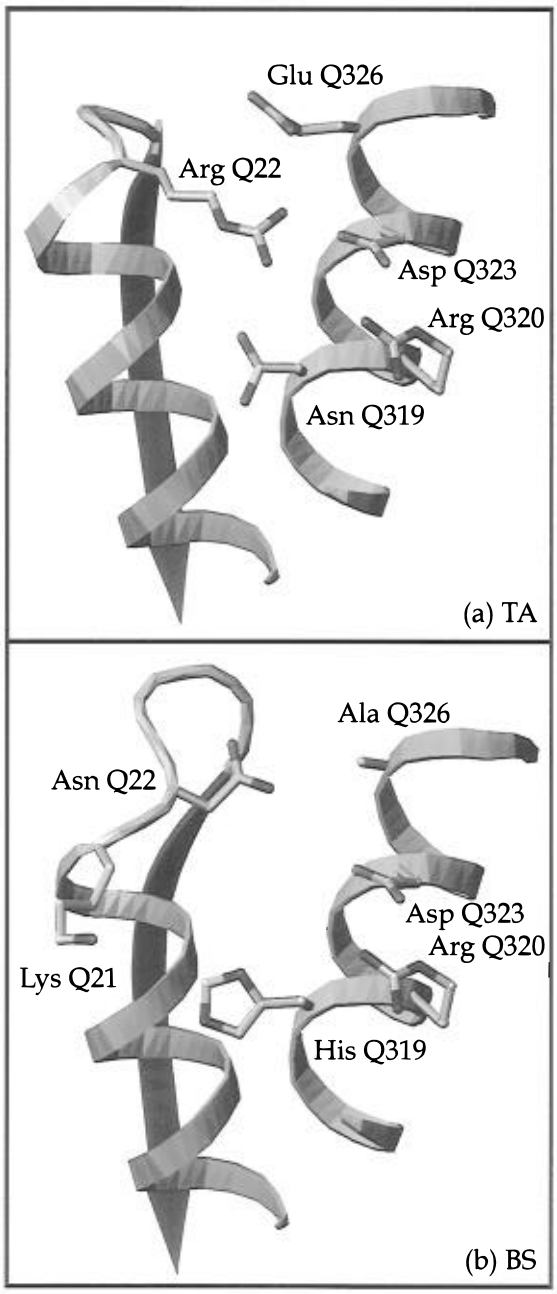

FIGURE 6: Comparison of the (a) TA and (b) BS structures in the region of the 20's loop of the Q subunit. The four-residue salt link network in TA joins different elements of secondary structure. These salt links are also present in the other three subunits. To place this figure in the context of the tetramer, see the arrow in Figure 1. The orientation of this figure differs from that of Figure 1.

149 during catalysis. The active-site regions of TA and BS were compared by superimposing residues within 5 Å of either Cys 149 or His 176. The resulting RMSD is less than 0.6 Å, suggesting that the active-site regions are structurally similar. This conclusion is confirmed with visual inspection. Furthermore, the NAD^+−protein interactions and the conformation of the NAD^+ molecules are virtually identical in BS and TA.

One possible significant difference between active-site regions of BS and TA is an additional hydrogen bond near the active site of the TA structure (Figure 7). Residues Cys 153 and Val 240 of BS are both replaced by Ser in TA. We observe a hydrogen bond between these Ser residues, with the OG−OG distance being 3.3 Å. Note that catalytic Cys

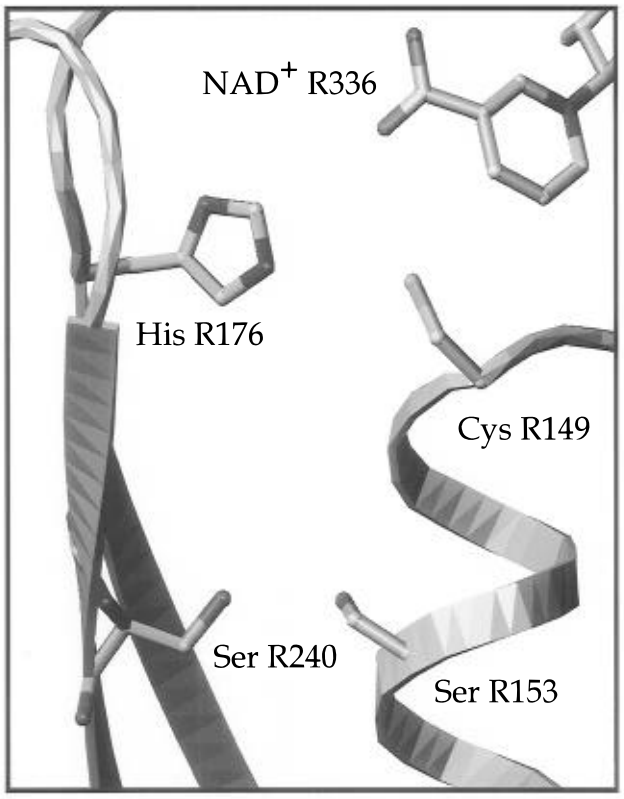

FIGURE 7: Ser 153−Ser 240 hydrogen bond in the active-site region of the R subunit. The active site residues Cys 149 and His 176 and the coenzyme NAD^+ are shown. The distance between the OG atoms of the two Ser residues is 3.3 Å. This hydrogen bond is also present in the other three subunits. For reference, the active-site regions are marked by the black spheres in Figure 1.

149 is located at the N-terminus of the helix that contains Ser 153. The Ser−Ser hydrogen bond links this helix to a β-strand, and perhaps provides some stabilization of the active-site region. Curiously, these residues are Ser and Thr in TM (Figure 4), and that structure also shows these residues to be within hydrogen bonding distance (2.8 Å). This hydrogen bond is not present in the HA structures because the HA sequence, like the BS sequence, has Cys 153 and Val 240.

(C) Phosphate Sites. Holo GAPDH structures determined from crystals grown in ammonium sulfate contain two sulfate molecules per subunit. These sulfates represent the substrate and inorganic phosphates involved in catalysis. Since our crystals were grown in poly(ethylene glycol) and 2-propanol, the phosphate sites are unoccupied, although there is weak positive difference density in some of the phosphate sites. We tried to model water molecules in one of these sites, but the *B*-factors refined to unreasonably large values. Thus, the sites are vacant in the present model.

The absence of sulfates causes three changes near the substrate phosphate site (residue SO_4 338 in BS). The side chain of Asp 181 is torsioned so that it moves toward the vacant substrate phosphate site, enabling it to hydrogen bond to Thr 179. There is continuous electron density connecting OD1 and OG1. The side chains of Arg 195 and Arg 231 are torsioned away from the vacant substrate phosphate site and make salt links to Asp 181, with distances of 3.5−4.0 Å. Whereas these distances are indicative of salt links, the electron density suggests that the strongest interaction is the hydrogen bond between Thr 179 and Asp 181.

Table 3: GAPDH Structures Compared in This Study

	HAH	HAA	BS	TA	TM
resolution (Å)	2.9	2.8	1.8	2.5	2.5
half-life at 100 °C (min)	<1	<1	<1	30	60
optimum growth temp of organism (°C)	20	20	58	70−75	80
sequence identity to TA	50	50	63	100	62

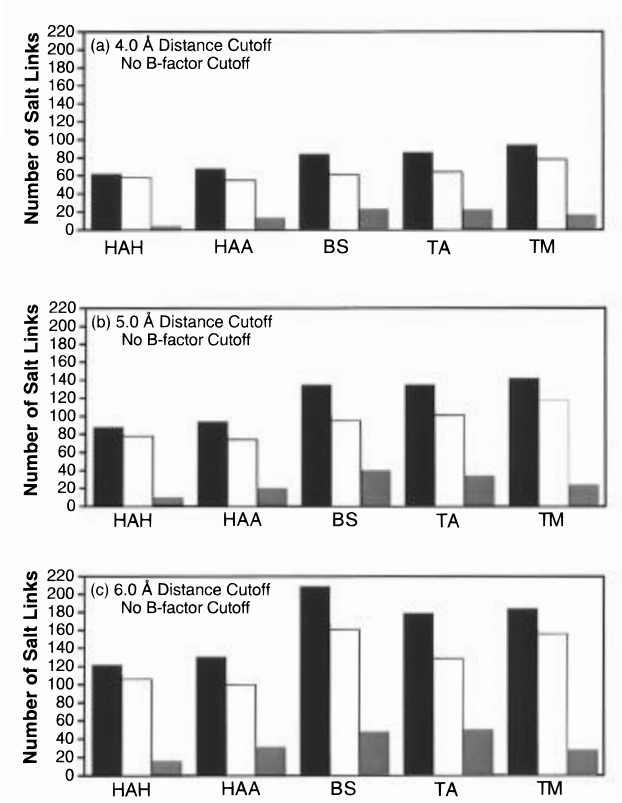

FIGURE 8: Bar graphs showing the number of salt links in the five GAPDHs compared in this study for various values of the interatomic cutoff distance. The black bars represent all salt links in the tetramer, the white bars represent intrasubunit salt links, and the gray bars represent intersubunit salt links.

Structural Basis of Thermostability. We next compare five GAPDH structures in terms of several quantities related to thermostability. The resolution of these structures, their sequence identity to TA, and some thermostability data are listed in Table 3. Note that both holo HA (HAH) and apo HA (HAA) are used in our comparison. HAH is used because BS, TA, and TM are also holo forms of the enzyme. We include HAA to minimize artifacts that could arise from the limited resolution of the HAH structure and the fact that the complete tetramer of HAH had to be built using NCS. The latter issue could have an effect on properties involving intersubunit interactions and buried and exposed surface area.

Salt Links. Salt links were identified using an interatomic distance cutoff applied to the carboxylate oxygen atoms of Glu and Asp; NE, NH1, and NH2 of Arg; NZ of Lys; and ND1 and NE2 of His. His residues 108, 141, 142, and 190 of our structure could be uncharged because the ND1 atoms appear to act as nucleophiles in hydrogen bonds. These His residues were also identified as possibly neutral in the BS structure, but no such analysis was made in the other GAPDH structures. Therefore, to obtain a fair comparison of the different structures, all His residues were assumed to be charged. In addition to a distance cutoff, we introduced a *B*-factor cutoff, in which atoms with high *B*-factors were

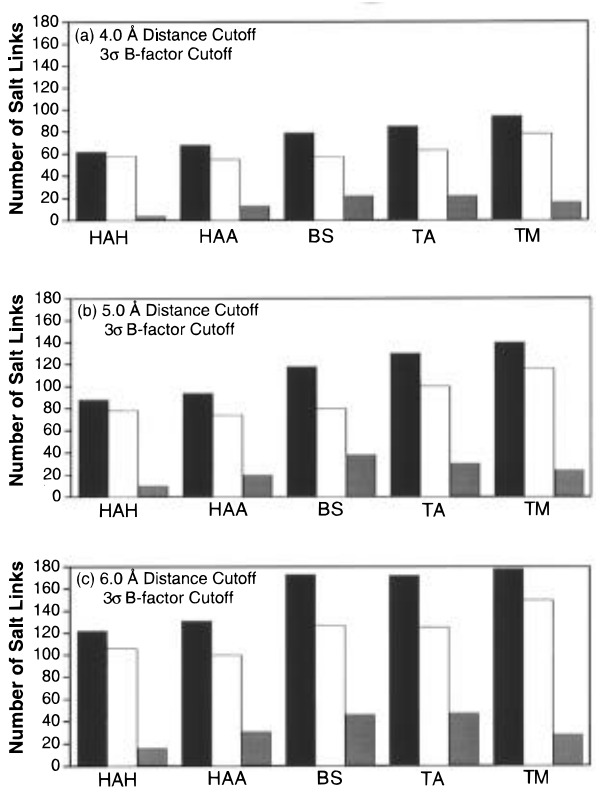

FIGURE 9: Bar graphs showing the number of salt links in the five GAPDHs compared in this study for various values of the interatomic cutoff distance and using a 3σ *B*-factor cutoff. The *B*-factor cutoff excludes atoms with *B* greater than 3σ above the mean of the respective structure. The black bars represent all salt links in the tetramer, the white bars represent intrasubunit salt links, and the gray bars represent intersubunit salt links.

omitted from the analysis. Since the *B*-factor is a measure of the positional uncertainty, a *B*-factor cutoff provides a way to select meaningful salt links.

The effects of distance and *B*-factor cutoffs on the number of salt links for the various GAPDH structures are shown in Figures 8 and 9. In Figure 8, we plot the number of salt links using various distance cutoff values, without the use of a *B*-factor cutoff. We observe several trends that are independent of the cutoff value. First, the total number of salt links in either of the three thermophiles is higher than in the psychrophile. Second, the thermophiles have more intrasubunit salt links than the psychrophile. Third, the moderate thermophile (BS) has the most intersubunit salt links, that is, more than HAH, HAA, TA, or TM. It appears, therefore, that the thermophiles may be discriminated from the psychrophile on the basis of the number of intrasubunit salt links, but not on the basis of intersubunit salt links. This observation is in agreement with Korndörfer et al. (1995).

The trends observed within the group of three thermophiles are not as clear. If the cutoff of 4.0−5.0 Å is used, TM has the most salt links, and BS and TA have about equal numbers of both total salt links and intrasubunit salt links (Figure 8). BS, however, has the most salt links of all the structures if a 6.0 Å cutoff is used. Thus, the correlation between the thermostability of the thermophiles and the number of salt links is somewhat dependent on the value of the distance cutoff.

If *B*-factor and distance cutoffs are used together, then both the total number of salt links and the number of intrasubunit salt links increase with increasing thermostability

for distance cutoffs of 4−5 Å (Figure 9a,b). A 6.0 Å cutoff yields almost equal numbers of salt links for the three thermophiles, with TM having the most salt links. The *B*-factor cutoff used in Figure 9 removes atoms with a *B*-factor greater than 3σ above the mean for the respective structure from the analysis. The 3σ *B*-factor cutoffs are 36.4 Å^2 for HAA, 53.9 Å^2 for BS, 64.6 Å^2 for TA, and 54.6 Å^2 for TM. A *B*-factor cutoff was not used for HAH since all atoms have a *B*-factor of zero.

Hydrogen Bonds. The hydrogen bond data shown below were calculated using a distance cutoff of 3.5 Å, an angle cutoff of 90° (linear hydrogen bond has angle 0° in this convention), and a 3σ *B*-factor cutoff (Baker & Hubbard, 1984). The distance cutoff was applied to the distance between the heavy atom donor and heavy atom acceptor atoms. The angle formed by the heavy atom acceptor, the hydrogen, and the heavy atom donor was subjected to the cutoff. To test the reliability of our results, we repeated the calculations using distance cutoffs in the range of 3.0−4.0 Å and angle cutoffs in the range of 60−90°. We found that the trends were independent of the cutoff values, provided a 3σ *B*-factor cutoff was used (data not shown).

Since the angle cutoff depends on the hydrogen atom positions, the number of hydrogen bonds will be sensitive to the method used to add hydrogen atoms to the crystal structure. Specifically, the hydrogen bonding observed depends upon whether one employs electrostatic and van der Waals forces during the generation of hydrogen atoms. To make a fair comparison, we added hydrogen atoms using X-PLOR with nonbonded forces turned on. In the previously solved structures, hydrogen atoms were added to the structures obtained from the data bank. For our structure, we removed the hydrogen atoms from the final model that was output from X-PLOR refinement, and then added back the hydrogen atoms with the same procedure used for the data bank structures.

The number of hydrogen bonds is shown in Figure 10. Both the total number of hydrogen bonds and the number of intrasubunit hydrogen bonds correlate with thermostability (Figure 10a). These trends are clearer if main chain hydrogen bonds are omitted from the analysis (Figure 10b).

To understand the basis for the correlation between thermostability and the number of hydrogen bonds, we classified each hydrogen bond involving a side chain atom as either "neutral-neutral" or "charged-neutral". We define a neutral-neutral hydrogen bond as a hydrogen bond between a side chain atom of a neutral residue and either a main chain atom of any residue or a side chain atom of another neutral residue. A charged-neutral hydrogen bond has a side chain atom of a charged residue as one partner, while the other partner is either a main chain atom of any residue or a side chain atom of a neutral residue.

We find that the structures contain nearly equal numbers of neutral-neutral hydrogen bonds, and these hydrogen bonds are not correlated with thermostability (data not shown). On the other hand, the number of charged-neutral hydrogen bonds correlates well with thermostability (Figure 10c). In fact, the correlation between thermostability and charged-neutral hydrogen bonding is stronger than the correlation between thermostability and the number of salt links (compare Figure 9b and Figure 10c). This trend is also observed if atoms involved in salt links are omitted from the calculation of hydrogen bonds, indicating that our observations are not simply a manifestation of the correlation between salt links and thermostability (data not shown).

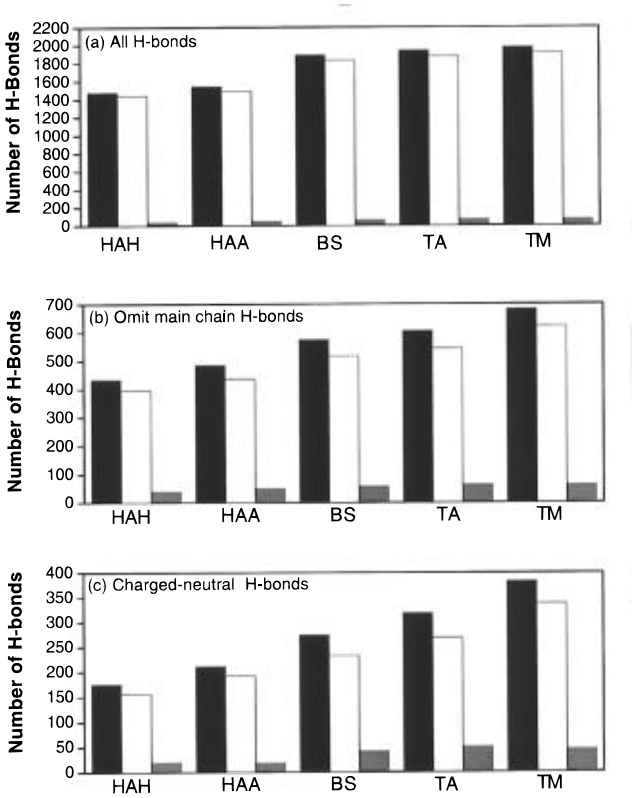

FIGURE 10: Bar graphs showing the number of hydrogen bonds in the five GAPDHs compared in this study. All hydrogen bonds are included in (a). All hydrogen bonds except main chain hydrogen bonds are shown in (b). In (c), only hydrogen bonds between a side chain atom of a charged residue and either a main chain atom of any residue or a side chain atom of a neutral residue are shown. In each graph, the black bars represent the sum of intrasubunit and intersubunit hydrogen bonds, the white bars represent intrasubunit hydrogen bonds, and the gray bars represent intersubunit hydrogen bonds.

Solvent-Accessible Surface Area (A_s). The total A_s of the tetramer and the A_s buried in the tetramer are listed in Table 4. The buried A_s was calculated by comparing the A_s of residues in the folded protein to values in a standard unfolded state (Miller et al., 1987). We also list the contributions to the buried A_s from hydrophobic, polar, and charged residues.

The thermophiles expose less surface area to solvent than the psychrophiles; however, the A_s is not strictly correlated with thermostability since the A_s of TM is between that of BS and HAA (see Table 4). On the other hand, we do observe a correlation between the total amount of buried A_s and thermostability. The breakdown of the buried A_s into residue types shows that the thermophiles bury more area than the psychrophile primarily in the form of charged residues. The buried A_s in the thermophiles from charged residues exceeds that of the psychrophiles by about 20%. The thermophiles also bury slightly (2−3%) more hydrophobic area than the psychrophiles. In contrast, the psychrophiles bury equal or greater A_s from polar residues than the thermophiles.

Packing Density and Surface to Volume Ratio. The packing density and surface to volume ratio are listed in Table 4. The packing density is defined as the ratio of the van der Waals volume to the volume enclosed by the molecular surface. The surface to volume ratio is the ratio

Table 4: Properties Related to Solvent-Accessible and Molecular Surfaces

	HAH	HAA	BS	TA	TM
A_s of tetramer (Å^2)	45 615	44 039	41 711	41 031	42 314
A_s buried in tetramer (Å^2)	169 129	170 704	174 781	175 397	176 430
A_s buried by hydrophobic residues (Å^2)[a]	84 728	85 186	86 869	88 860	86 143
A_s buried by polar residues (Å^2)[a]	36 108	36 529	35 615	33 748	36 606
A_s buried by charged residues (Å^2)[a]	38 329	39 105	46 026	46 753	46 201
packing density	0.65	0.65	0.64	0.64	0.64
surface to volume ratio (Å^{-1})	0.27	0.24	0.21	0.21	0.21
area of molecular surface (Å^2)	45 982	40 824	37 518	36 541	37 813
vol enclosed by molecular surface (Å^3)	171 208	171 581	178 802	175 873	178 921

[a] Hydrophobic includes Ala, Val, Ile, Leu, Met, Phe, Trp, and Pro. Polar includes Tyr, Asn, Gln, Ser, and Thr. Charged includes Asp, Glu, Arg, Lys, and His.

of the area of the molecular surface to the volume enclosed by the molecular surface.

We do not observe an increase in the packing density with increasing thermostability. Rather, the structures have equal packing densities, within the accuracy of these calculations. We do see a decrease in the surface to volume ratio with increasing thermostability. This decrease is due in part by small increases in the volume enclosed by the molecular surface, but it is mostly due to larger decreases in the area of the molecular surface (see Table 4).

Stabilization of α-Helices and β-Turns. We compared the amino acid composition of the helices in the four GAPDHs, assuming that stabilizing substitutions conserved in the three thermophiles but not in the psychrophile were important for thermostability (see Figure 4). We find that the 40's helix in the three thermophiles could be stabilized by the Val to Ala substitution at position 41 and the Ala to Asp substitution at position 36. The former sequence change occurs in the middle of this helix, and the latter occurs at the helix N-terminus. There is a hydrogen bond between the side chain of Asp 36 and either the main chain N or the OG1 of Thr 39 in all three thermophiles, indicating that Asp 36 is not interacting with the helix dipole (Nicholson et al., 1988). Since only two putative stabilizing substitutions are found, we doubt that helix stabilization is playing a major role in the thermostability of these GAPDHs.

A Pro at position 2 of a β-turn can be stabilizing (Watanabe et al., 1994). The five GAPDH structures each contain four such Pro residues; therefore, this motif does not account for the observed differences in thermostability. Pro 79 and Pro 219 are conserved in all the structures, while Pro 138A is conserved only in the three thermophiles. Pro 266 occurs only in HA and TA, and Pro 23 occurs in only in BS and TM. Pro 33 is observed only in HA. These residues are in type III β-turns, except for Pro 266 of HA and TA and Pro 23 of TM, which are type I turns.

Sequence Conservation. The above analyses focused on a comparison of either the number of stabilizing interactions (salt links, hydrogen bonds, etc.) found in the GAPDH structures or a global property such as the packing density or the surface to volume ratio. An alternative scheme is to use sequence conservation as a guide to locating regions of the protein that may be conferring stabilization. With the addition of the TA structure, we now have the structures of two highly thermostable GAPDHs (TA and TM) with which to perform such an analysis.

The residues marked by the boxes in the sequence alignments in Figure 4 are conserved in TA and TM, but not in either HA or BS. There are 21 such residues. We examined the structural context of these residues to see if any were involved in possibly stabilizing motifs. We find that several of these conserved residues are involved in salt links, hydrogen bonds, and hydrophobic interactions.

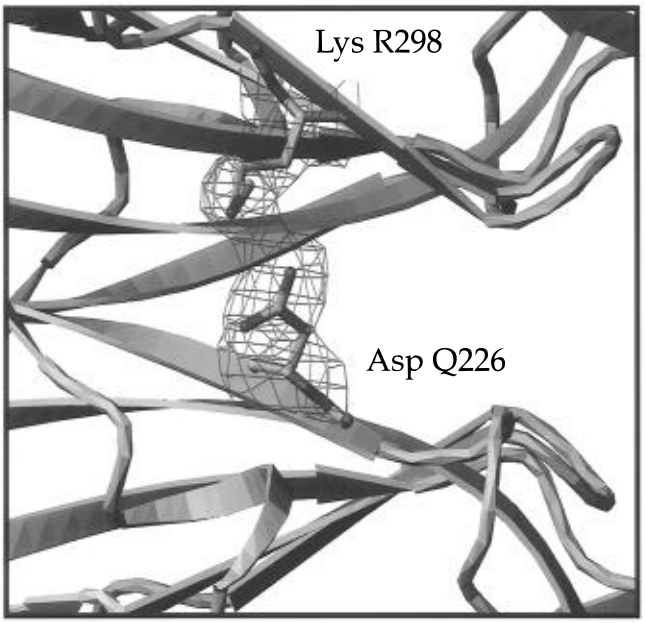

FIGURE 11: Lys R298−Asp Q226 salt link of TA. The NCS-averaged, solvent-flattened, $|F_o|$ map is contoured at 1σ. This figure is a magnified view of the boxed region of Figure 1. The orientation of this figure is identical to that of Figure 1.

Among all the salt links found in TA and TM, only two are present in both TA and TM, but absent in HA and BS: Arg 22−Glu 326 and Arg 22−Asp 323. These salt links were discussed in a previous section (see Figure 6). Arg 22 is replaced by Lys in BS and Cys in HA. Glu 326 is replaced by Ala in BS and Lys in HA. Furthermore, Asn 319 could be implicated in the formation of these salt links (see discussion above), and it too is conserved only in TA and TM. We note that the Arg 22−Glu 326 salt link was predicted in a modeling study of TA; however, the Arg 22−Asp 323 salt link was not part of that model structure (Walker et al., 1980).

Cys 153 of HA and BS are replaced by Ser in TA and TM. Ser 153 was discussed in the section on the comparison of the active sites of BS and TA (see Figure 7). Ser 153 makes a hydrogen bond to Ser 240 in TA and to Thr 240 in TM. Note also from Figure 4 that residue 240 is Val in HA and BS. Thus, both hydrogen bond partners are conserved only in TA and TM.

Asp 226 is conserved only in TA and TM. This residue is Thr in HA and Asn in BS. In TA, Asp 226 forms an

intersubunit salt link with Lys 298 (Figure 11). This interaction links subunits related by the P molecular axis, and there are four such salt links per tetramer: O226−P298, P226−O298, Q226−R298, R226−Q298. All four salt links are observed in TA. These intersubunit salt links were predicted in a model structure of TA (Walker et al., 1980). In TM, Asp 226 forms an intersubunit hydrogen bond to Asn 298, if the χ_2 dihedral angle of Asn 298 is rotated by 180°. This rotation does not create a steric clash, nor does it disrupt an existing hydrogen bond. It seems, therefore, that an intersubunit interaction in this region is conserved only in TA and TM. Although our data indicate that intersubunit salt links are not correlated with thermostability, this particular intersubunit interaction is present in both TA and TM, and thus could be important.

There are several sequence changes of the type Ala→Ile, Val→Ile, and Ser→Thr that increase the side chain branching in TA and TM, relative to HA and BS. For example, consider Ile 18, Ile 30, Ile 93, Thr 119, Ile 143, Ile 239, and Ile 278 of TA or TM (Figure 4). These residues are buried in TA and TM, with A_s less than 8%. Mutation to Ile and Thr increases the amount of surface area buried by these residues, and thus could be a source of hydrophobic stabilization.

DISCUSSION

Salt Links and Hydrogen Bonds. We find a clear correlation between the number of hydrogen bonds and thermostability in the GAPDHs studied. This correlation is quite strong if only charged-neutral hydrogen bonds are considered. Although a hydrogen bond may contribute from 0.5 to 2 kcal/mol to the free energy of stabilization (Fersht, 1972; Anderson et al., 1990; Horovitz et al., 1990; Dao-pin et al., 1991; Sali et al., 1991; Shirley et al., 1992; Fersht & Serrano, 1993; Waldburger et al., 1995), their role in thermophilic proteins is seldom discussed. Presumably this is because of their large numbers and the difficulty in determining which of them are important in any given structure. Note that the thermophilic GAPDHs have hundreds more hydrogen bonds than the psychrophilic GAPDH. If each extra hydrogen bond contributed the expected amount to the energy of stabilization, then the free energy of these enzymes would far exceed their experimental values.

Since we observe that thermostability correlates strongly with charged-neutral hydrogen bonds, they may be more important than other hydrogen bonding pairs. There are two reasons that proteins may use charged-neutral hydrogen bonds rather than salt links or neutral-neutral hydrogen bonds to stabilize proteins. First, the desolvation penalty associated with burying a charged-neutral hydrogen bond would be less than that of a salt link because only one charged residue is involved. Second, the enthalpic reward of a charged-neutral hydrogen bond is greater than that of a neutral-neutral hydrogen bond because of the charge-dipole interaction. These ideas could be tested with double mutant cycle experiments and continuum electrostatics theories. Our results with charged-neutral hydrogen bonds are independent of distance and angular cutoffs used in the calculation and indicate to us that the role of charged residues in stabilizing thermophilic proteins may not be limited to the formation of salt links.

We also find that the number of intrasubunit salt links correlates with thermostability; however, this correlation is not as strong as the one involving charged-neutral hydrogen bonds. These results are also independent of the distance cutoff used to define a salt link, provided that atoms with large *B*-factors are omitted from the analysis. The situation regarding intersubunit salt links is not as clear. Whereas the three thermophiles have more intersubunit salt links than the psychrophile, within the group of three thermophiles the number of intersubunit salt links is inversely correlated with thermostability.

In comparisons between crystal structures solved at different times in different laboratories, one concern is that the reported differences in numbers of electrostatic interactions are due to variations in refinement software and strategy. For example, some refinement programs use force fields that include not only bond, angle, and dihedral terms, but also nonbonded electrostatic terms based on partial charges. The degree to which the observed salt links and hydrogen bonds are biased by the force field parameters, data collection, and processing and refinement is not known. We worked to avoid this bias in our comparison by adding polar hydrogens to all of the structures in a uniform manner using the same software. Next, we employed a *B*-factor cutoff in these calculations which eliminated atoms with less positional reliability. More importantly, we calculated these bonds using different distance and angle cutoffs and only reported findings that were invariant to the method of calculation.

Nevertheless, the detailed nature of the questions now being asked in the studies of thermophilic enzymes could require that similar force fields and refinement programs be used in structure analysis. These concerns are expected to be minimized at higher resolution, suggesting a need for new higher resolution structures of both thermophilic and mesophilic enzymes.

Hydrophobic Interactions. To investigate the role of hydrophobic interactions in GAPDH, we calculated several properties related to the burial of A_s. While the thermophiles bury only slightly more A_s from hydrophobic residues than the psychrophile, they bury significantly more A_s from charged residues than the psychrophile. This result is consistent with our observations that the thermophiles have more salt links and charged-neutral hydrogen bonds than the psychrophile. If the total surface area buried by hydrophobic residues is a good measure of the stabilization provided by the hydrophobic effect, then it appears that the stability of the thermophilic GAPDHs derives more from electrostatic interactions (salt links and hydrogen bonds) than hydrophobic interactions.

Packing Density and Surface to Volume Ratio. Our analyses show the packing densities of the five GAPDH structures to be nearly identical. In contrast, the surface to volume ratios of the thermophiles are about 12−22% smaller than that of the psychrophile. While it has been suggested that decreased surface to volume ratio is related to thermostability (Chan et al., 1995), the physical basis of this relationship has not been elucidated. Our calculations offer some insight as to why a decrease in the surface to volume ratio can be stabilizing.

Decreases in the surface to volume ratio in our study result from both an increase in the volume enclosed by the molecular surface and a decrease in the area of the molecular

surface. One way for a three-dimensional object to decrease its surface area and increase its volume is to become more spherical.

Consider the protein and solvent to be two phases, like a drop of oil in water. To bring a residue from the bulk of the protein to the surface, that is, to create a new surface, work must be done against the cohesive forces in the protein. This work is proportional to the change in the surface area for this process, with the constant of proportionality being the surface tension (Moore, 1972). In this model, a spherical protein would minimize the surface area and maximize the number of residues in the interior of the protein. A consequence of this notion is that maximization of the cohesive forces *inside* the protein is driving the tendency toward a more spherical protein. Therefore, buried salt links, buried hydrogen bonds, and hydrophobic interactions are more likely to confer thermostability than are interactions on the surface such as solvent-exposed salt links. Mutation studies (Matthews, 1991) and an analysis of the conservation of salt links in protein families (Schueler & Margalit, 1995) support the idea that buried residues, rather than surface residues, are responsible for stability.

Stabilization of α-Helices and β-Turns. We inspected helices for increased Ala content and for helix dipole stabilization, and found only two examples of these elements in thermophilic GAPDHs. Likewise, the GAPDH structures compared here have the same number of Pro residues at position 2 in β-turns. Therefore, we conclude that these motifs are not playing a major role in the stabilization of thermophilic GAPDHs relative to the psychrophile, nor do they account for the relative thermostabilities of the three thermophiles.

Sequence Conservation. The notion that increased thermostability results from an amalgam of many small changes throughout the enzyme is the basis for analyses such as calculating the total number of salt links, hydrogen bonds, buried surface area, and surface to volume ratio. Another view is that a few specific interactions account for thermostability. This view forms the basis for mutational studies designed to alter an enzyme's thermostability.

We investigated this idea by assuming that residues that were contributing significantly to thermostability were also conserved in the two most thermostable GAPDHs. Analysis of the 21 such residues that are conserved only in TA and TM revealed 2 conserved intrasubunit salt links involving Arg 22, 1 conserved intrasubunit hydrogen bond near the active site involving Ser 153, and 1 intersubunit site that is occupied by a salt link in TA and a hydrogen bond in TM. In addition, we found seven buried residues (six Ile and one Thr) that could contribute to thermostability by increasing the amount of buried surface area and therefore could provide stabilization via the hydrophobic effect.

The fact that certain salt links and hydrogen bonds are conserved in TA and TM is consistent with our finding that thermostability is correlated with the overall number of salt links and hydrogen bonds. The conservation of several buried Ile residues is an interesting result because neither the packing density nor the A_s buried by hydrophobic residues is strongly correlated with thermostability. The influence of these residues on thermostability is being addressed with mutational studies.

ACKNOWLEDGMENT

We thank George Phillips for the use of the R-AXIS detector at Rice University, Ingo Korndörfer for useful discussions, and Mitch Miller for help with preparing figures.

REFERENCES

Abola, E. E., Bernstein, F. C., Bryant, S. H., Koetzle, T. F., & Weng, J. (1987) in *Crystallographic databases—Information content, software systems, scientific applications* (Allen, F. H., Bergerhoff, G., & Sievers, R., Eds,) pp 107−132, Data Commission of the International Union of Crystallography, Bonn/Cambridge/Chester.

Adams, M. W. W., & Kelly, R. M. (1994) *Bioorg. Med. Chem. 2*, 659−667.

Alber, T. (1989) *Annu. Rev. Biochem. 58*, 765−798.

Anderson, D. E., Becktel, W. J., & Dahlquist, F. W. (1990) *Biochemistry 29*, 765−784.

Argos, P., Rossmann, M. G., Grau, U. M., Zuber, H., Frank, G., & Tratschin, J. D. (1979) *Biochemistry 18*, 5698−5703.

Baker, E. N., & Hubbard, R. E. (1984) *Prog. Biophys. Mol. Biol. 44*, 97−179.

Biro, J., Fabry, S., Dietmaier, W., Bogedain, C., & Hensel, R. (1990) *FEBS Lett. 275*, 130−134.

Brünger, A. T. (1992) *X-PLOR version 3.1, A system for x-ray crystallography and NMR*, Yale University Press, New Haven.

Chan, M. K., Mukund, S., Kletzin, A., Adams, M. W. W., & Rees, D. C. (1995) *Science 267*, 1463−1469.

Dao-pin, S., Sauer, U., Nicholson, H., & Matthews, B. W. (1991) *Biochemistry 30*, 7142−7153.

Davies, G. J., Gamblin, S. J., Littlechild, J. A., & Watson, H. C. (1993) *Proteins: Struct., Funct., Genet. 15*, 283−289.

Day, M. W., Hsu, B. T., Joshua-Tor, L., Park, J.-B., Zhou, Z. H., Adams, M. W. W., & Rees, D. C. (1992) *Protein Sci. 1*, 1494−1507.

Devereux, J., Haeberli, P., & Smithies, O. (1984) *Nucleic Acids Res. 12*, 387−395.

Engh, R. A., & Huber, R. (1991) *Acta Crystallogr. A47*, 392−400.

Fabry, S., Lang, J., Niermann, T., Vingron, M., & Hensel, R. (1989) *Eur. J. Biochem. 179*, 405−413.

Fersht, A. R. (1972) *J. Mol. Biol. 64*, 497−509.

Fersht, A. R., & Serrano, L. (1993) *Curr. Opin. Struct. Biol. 3*, 75−83.

Furey, W., & Swaminathan, S. (1995) in *Macromolecular Crystallography, A Volume of Methods in Enzymology* (Carter, C., & Sweet, R., Eds.) Academic Press, Orlando, FL.

Griffith, J. P., Lee, B., Murdock, A. L., & Amelunxen, R. E. (1983) *J. Mol. Biol. 169*, 963−974.

Hendsch, Z. S., & Tidor, B. (1994) *Protein Sci. 3*, 211−226.

Higashi, T. (1990) *PROCESS: A program for indexing and processing R-AXIS II imaging plate data*, Rigaku Corp., Tokyo.

Honig, B., & Nicholls, A. (1995) *Science 268*, 1144−1149.

Honka, E., Fabry, S., Niermann, T., Palm, P., & Hensel, R. (1990) *Eur. J. Biochem. 188*, 623−632.

Horovitz, A., Serrano, L., Avron, B., Bycroft, M., & Fersht, A. R. (1990) *J. Mol. Biol. 216*, 1031−1044.

Jaenicke, R. (1991) *Eur. J. Biochem. 202*, 715−728.

Jecht, M., Tomschy, A., Kirschner, K., & Jaenicke, R. (1994) *Protein Sci. 3*, 411−418.

Jones, T. A. (1978) *J. Appl. Crystallogr. 11*, 268−272.

Jones, T. A., Zou, J.-Y., Cowan, S. W., & Kjeldgaard, M. (1991) *Acta Crystallogr. A47*, 110−119.

Kelly, C. A., Bishiyama, M., Ohnishi, Y., Beppu, T., & Birktoft, J. J. (1993) *Biochemistry 32*, 3913−3922.

Knapp, S., Karshikoff, A., Waldkötter, K., Rüdiger, A., Antranikian, G., & Ladenstein, R. (1995) *Acta. Crystallogr. D51*, 395−398.

Korndörfer, I., Steipe, B., Huber, R., Tomschy, A., & Jaenicke, R. (1995) *J. Mol. Biol. 246*, 511−521.

Kotik, M., & Zuber, H. (1993) *Eur. J. Biochem. 211*, 267−280.

Laskowski, R. A., MacArthur, M. W., Moss, D. S., & Thornton, J. M. (1993) *J. Appl. Crystallogr. 26*, 283−291.

Lin, Z.-j., Li, J., Zhang, F.-m., Song, S.-y., Yang, J., Liang, S.-j., & Tsou, C.-l. (1993) *Arch. Biochem. Biophys. 302*, 161−166.

Luzzati, P. V. (1952) *Acta Crystallogr. 5*, 802−810.
Matthews, B. W. (1991) *Curr. Opin. Struct. Biol. 1*, 17−21.
Matthews, B. W. (1995) *Annu. Rev. Biochem. 62*, 139−160.
Menendez-Arias, L., & Argos, P. (1989) *J. Mol. Biol. 206*, 397−406.
Mercer, W. D., Winn, S. I., & Watson, H. C. (1976) *J. Mol. Biol. 104*, 277−283.
Merkler, D. J., Farrington, G. K., & Wedler, F. C. (1981) *Int. J. Pept. Protein Res. 18*, 430−442.
Miller, S., Janin, J., Lesk, A. M., & Chothia, C. (1987) *J. Mol. Biol. 196*, 641−656.
Moore, W. J. (1972) *Physical Chemistry*, Prentice-Hall, Englewood Cliffs, NJ.
Moras, D., Olsen, K. W., Sabesan, M. N., Buehner, M., Ford, G. C., & Rossmann, M. G. (1975) *J. Biol. Chem. 250*, 9137−9162.
Murthy, M. R. N., Garavito, R. M., Johnson, J. E., & Rossmann, M. G. (1980) *J. Mol. Biol. 138*, 859−872.
Nicholls, A., & Honig, B. (1992) *GRASP: graphical representation and analysis of surface properties*, Columbia University, New York.
Nicholson, H., Becktel, W. J., & Matthews, B. W. (1988) *Nature 336*, 651−656.
Perutz, M. F., & Raidt, H. (1975) *Nature 255*, 256−259.
Rees, D. C., & Adams, M. W. W. (1995) *Structure 3*, 251−254.
Rehaber, V., & Jaenicke, R. (1992) *J. Biol. Chem. 267*, 10999−11006.
Sali, D., Bycroft, M., & Fersht, A. R. (1991) *J. Mol. Biol. 220*, 779−788.
Schläpfer, B. S., & Zuber, H. (1992) *Gene 122*, 53−62.
Schueler, O., & Margalit, H. (1995) *J. Mol. Biol. 248*, 125−135.
Shirley, B. A., Stanssens, P., Hahn, U., & Pace, C. N. (1992) *Biochemistry 31*, 725−732.
Skarzynski, T., & Wonacot, A. J. (1988) *J. Mol. Biol. 203*, 1097−1118.
Skarzynski, T., Moody, P. C. E., & Wonacott, A. J. (1987) *J. Mol. Biol. 193*, 171−187.
Sterner, R., Vogl, T., Hinz, H.-J., Penz, F., Hoff, R., Föll, R., & Decker, H. (1995) *FEBS Lett. 364*, 9−12.
Suzuki, K., & Harris, J. I. (1971) *FEBS Lett. 13*, 217−220.
Tanner, J., & Krause, K. L. (1994) *Rigaku J. 11*, 4−10.
Tanner, J., Hecht, R. M., Pisegna, M., Seth, D. M., & Krause, K. L. (1994) *Acta Crystallogr. D50*, 744−748.
Tomschy, A., Bohm, G., & Jaenicke, R. (1994) *Protein Eng. 7*, 1471−1478.
Tomschy, A., Glockshuber, R., & Jaenicke, R. (1993) *Eur. J. Biochem. 214*, 43−50.
Vellieux, F. M. D., Hajdu, J., Verlinde, C. L. M. J., Groendijk, H., Read, R. J., Greenhough, T. J., Campbell, J. W., Kalk, K. H., Littlechild, J. A., Watson, H. C., & Hol, W. G. J. (1993) *Proc. Natl. Acad. Sci. U.S.A. 90*, 2355−2359.
Waldburger, C. D., Schildbach, J. F., & Sauer, R. T. (1995) *Nat. Struct. Biol. 2*, 122−128.
Walker, J. E., Wonacott, A. J., & Harris, J. I. (1980) *Eur. J. Biochem. 108*, 581−586.
Watanabe, K., Masuda, T., Ohashi, H., Mihara, H., & Suzuki, Y. (1994) *Eur. J. Biochem. 226*, 277−283.
Yang, A.-S., Sharp, K. A., & Honig, B. (1992) *J. Mol. Biol. 227*, 889−900.
Yip, K. S. P., Baker, P. J., Britton, K. L., Engel, P. C., Rice, D. W., Sedelnikova, S. E., Stillman, T. J., Pasquo, A., Chiaraluce, R., Consalvi, V., & Scandurra, R. (1995) *Acta. Crystallogr. D51*, 240−242.
Zuber, H. (1981) in *Structural and functional aspects of enzyme catalysis* (Eggerer, H., & Huber, R., Eds.) pp 114−127, Springer-Verlag, Berlin.
Zwickl, P., Fabry, S., Bogedain, C., Haas, A., & Hensel, R. (1990) *J. Bacteriol. 172*, 4329−4338.

BI951988Q